Sensors and Actuators A 297 (2019) 111493

Contents lists available at ScienceDirect

Sensors and Actuators A: Physical

journal homepage: www.elsevier.com/locate/sna

Photonic crystal slab biosensors fabricated with helium ion lithography (HIL)

Yue Zhuo[a,b,c,1], Huan Hu[d,*,1], Yifei Wang[e], Thibault Marin[f], Meng Lu[e]

[a] Department of Bioengineering, University of Illinois at Urbana-Champaign, Urbana, IL 61801, USA
[b] Micro and Nanotechnology Laboratory, 208 North Wright Street, Urbana, IL 61801, USA
[c] Beckman Institute for Advanced Science & Technology, 405 N Mathews Ave, Urbana, IL 61801, USA
[d] ZJU-UIUC Institute, International Campus, Zhejiang University, Haining, Zhejiang 314400, China
[e] Department of Electrical and Computer Engineering, Iowa State University, Ames, IA 50011, USA
[f] Atkins Building, University of Illinois Research Park, 1800 S. Oak St., Champaign, IL 61820, USA

ARTICLE INFO

Article history:
Received 26 March 2019
Received in revised form 13 June 2019
Accepted 9 July 2019
Available online 26 July 2019

Keywords:
Photonic crystal biosensor
Helium ion lithography
Nanoimprint lithography
Nanofabrication
Rapid-prototyping

ABSTRACT

A photonic crystal slab is a periodic arranged dielectric nanostructure which can be used in many applications, such as a label-free optical biosensor. This work demonstrates a novel nanofabrication process using helium ion lithography (HIL) for the rapid prototyping of master molds, which can be repeatedly used for fabricating photonic crystal slabs by nanoimprint lithography. To prove the concept, photonic crystal slabs with nano-grating and nano-hole patterns have been fabricated and the results show that the photonic crystal slabs fabricated by the HIL in conjunction with the nanoimprint lithography demonstrate photonic bandgaps. The functional tests demonstrate that the fabricated nano structures can be utilized as refractometric sensors to detect changes of the refractive index caused by adsorption of biochemicals. This fabrication approach offers a new route for mass-production of high-quality photonic crystal biosensors with a variety of nano-patterns.

1. Introduction

Photonic crystals (PCs) are nanostructures with periodic arranged dielectric materials of the refractive indices. With photonic bandgaps in the nanostructure, the PC surface demonstrates high reflection efficiency with narrow bandwidth when the resonance condition is satisfied. Thanks to their ability to control and manipulate the flow of light, PCs have been utilized in promising applications in lasers, solar cells, light emitting diodes (LED), optical fibers, optical sensors and filters, mechanical stress sensing, and more [1–41].

To date, the economic mass-manufacturing of high-quality PCs over large surface remains challenging. Existing nanofabrication technology for PCs typically falls into two categories: bottom-up and top-down. The bottom-up approach typically uses the assembly of nanoparticles for building the PCs [42] or uses the self-assembled structures as molds [43–45]. Bottom-up approaches normally have lower-cost and can scale up to fabricate in large-area. But the PCs formed by bottom-up approaches are very limited in type and cannot have precise control in dimension and location. Top-down approaches, such as electron beam lithography (EBL) [46], focused ion beam lithography [47], Deep Utra-Violet Light Lithography (DUV) [48] and laser ablation [49], have better control in the nanopattern shape, dimension, and location, but are generally more expensive and more difficult to scale up. Moreover, these top-down methods generally have difficulty to mass-produce three-dimensional (3D) nanostructures including 3D PCs due to the limited penetration depth of the UV light.

Prior research on PCs also manifested the dependence of PCs' development on the fabrication technology. Although the concept of PCs and photonic stop-bands has been studied since Lord Rayleigh in 1887, mainly as *Bragg mirrors* in a form of a stack of one-dimensional (1D) periodic arranged refractive index materials [50], research for PCs is either theoretical only or in the microwave regime (structure with period in centimeter scales) due to the difficulty to efficiently fabricate periodic structures in optical regime (structure with period in sub-micrometer or nanometer scales) at earlier stages [1–3]. The research on PCs regained the momentum when the higher-dimensional PCs was proposed by Yablonovitch and John in 1987, separately [4,5]. These higher-dimensional PCs have 3D photonic bandgaps, critical for many applications [51], but the fabrication process is quite challenging requiring strict alignments and precise control over positions and sizes [52–59] beyond

* Corresponding author.
E-mail addresses: yuezhuo2@illinois.edu (Y. Zhuo), huanhu@intl.zju.edu.cn (H. Hu).
[1] These authors contributed equally to this paper.

https://doi.org/10.1016/j.sna.2019.07.017
0924-4247/

the fabrication capability of any single existing nanofabrication technology for mass-production.

An alternative way is to use a PC slab, which is another type of attractive structure since it is relatively easier to realize with known industry method at submicron scales. A PC slab can have 1D or two-dimensional (2D) periodicity and utilize the index guiding to confine the light in the 3rd dimension [7,60–66]. In 1996, Krauss et al. fabricated the first 2D PC slab in optical regime by utilizing methods from semiconductor fabrication [67]. The inspiring work enables the engineering of photonic dispersion in the slab using techniques from the semiconductor industry and fast-forwards the development of PC fabrication in optical regimes for mass-production. In 2002, Cunningham et al. fabricated a 1D plastic PC slab using nanoimprint lithography and demonstrated the application of such fabricated PC surface as a biosensor for label-free detection of biochemical interactions [12,13]. This low-cost fabrication method enables the easy mass-production of PC slab with high precision between chips and therefore has the potential to realize single-use disposable chips in industry. Today, this method has been utilized for many applications in biosensing and bioimaging to detect nanoparticles, analytes interactions, or cellular functions [30,68–70].

In this work, we demonstrate a new way to fabricate PC slab-based biosensors by combining helium ion lithography and nanoimprint lithography. Helium ion lithography (HIL) has recently been introduced by utilizing scanning helium ion microscope with high-brightness helium ions source focused at a small spot size and used to scan the substrate for lithography [71,72]. Comparing with EBL, HIL has two potential advantages: (1) HIL uses ions which are much heavier ($\sim 7 \times 10^3$ times) charged-particles than electrons and the shorter de Broglie wavelength results in less diffraction. The smaller apertures in HIL lead to the suppression of the spherical aberration and the angular spread of the helium ion beam. Therefore, the beam spot size is smaller in HIL. (2) With similar energy, the helium ions have smaller surface interaction volume and the energy loss has a smaller statistical spread since the higher momentum of helium ions resists space charge effects. Thus the smaller spot size and higher surface sensitivity significantly reduced proximity effect in HIL [73], which can offer higher-resolution lithography fabricating nanopatterns with better fidelity and resolution.

To transfer the nanopatterns from the mold to a target chip, a high-throughput and low-cost fabrication method is desired. Nanoimprint lithography (NIL), also named nanoreplica molding, uses a template to control the transformed patterns. NIL fabricates patterns in nanometer scales based on mechanical deformation of the curable polymer by heat or UV light and can achieve molecular-scale resolution [74–76]. Therefore, combining HIL and NIL to fabricate the PC slab can lead to high resolution, high throughput and low-cost lithography. To prove the concept, we utilized a nanofabrication process that directly uses a nanoscale poly(methyl methacrylate) (PMMA) nanograting mold patterned by HIL for the construction of a functional PC slab biosensor. With a simple replica molding step by NIL, the PMMA molds can repeatedly be used for constructing PCs made of UV-curable epoxy polymer (ZIPCONE™ UA PP1-ZPUA, Gelest, Inc.). We demonstrated PC slab surface nanopatterns with a period of ~400 nm and area of 600 μm × 600 μm showing good resonance peaks. The repel saline (PlusOne Repel-Silane ES, GE Healthcare) was applied on the surface of PMMA mold promote anti-adhesion and hexamethyldisilazane (HDMS) was applied on the substrate before nano-replica molding procedure to promote adhesion. With this fabrication approach, the PC slab biosensor can be potentially produced using HIL and NIL in a mass-scale production manner in the future.

2. Results and discussions

2.1. HIL dose test for PMMA Mold

To seek the optimal lithography condition, a helium ion dose test for PMMA mold was performed. Several circles with 400 nm diameter were exposed with different amount of He^+ ion doses. Dwelling time is chosen from 0.1 μs up to 800 μs covering a dose range from 0.1 to 80 ion/nm^2. Fig. 1(a) shows the Scanning Electron Microscope (SEM) images of PMMA nanostructures after developing. SEM images also show that above the thresholding dose (around 1 ion/nm^2), PMMA exhibits negative resist properties resulting into a center exposed region remaining rather than dissolved agreeing with reported work [73]. Fig. 1(b) plots the diameter of the hole at each dose. The dose-response can be fitted to an exponential curve ($\mathbf{y} = a \cdot e^{bx} + c$) with parameters of a = -175.62, b = -0.92, c = 626.04. The diameter of the developed hole increases linearly with dose in the beginning, and then gradually saturates at larger doses. Based on the dose test, 0.2 ions/nm^2 is chosen for all the device fabrication in this work. Exposing a 400 nm diameter hole leads to a PMMA hole with ~500 nm diameter at this dose level, which means that the actual dimension is ~100 nm larger than the desired pattern size and this is mainly due to forward scattering of the helium ions and secondary electrons exposures as pointed out by [77]. Although using thinner PMMA resist can lead to better lithography resolution, ~100 nm thick PMMA resist is chosen here to achieve the goal of directly adopting as the nanoimprint mold with the desired PC nanograting height. Such choice allows the elimination of the etching step and therefore speeds up the whole fabrication process.

Fig. 2 shows SEM images of the resulting PMMA mold fabricated with HIL (Fig. 2 Left column) and the final PC slab biosensors fabricated with NIL (Fig. 2 Right column). Fig. 2 (a, c) shows two types of 1D PMMA nanogratings with the same pitch (period) of 400 nm but with different duty-cycles (or grating-widths). These cross-sectional views also demostrate that the HIL-fabricated nanogratings exhibit a sharp edge in the corner of the structures with a grating-thickness of ~100 nm. Fig. 2(b) and (d) are the top-views of the corresponding replicated UV-Epoxy nanostructures. Fig. 2(e) and (f) show a PMMA mold and a UV-Epoxy structure of the 2D PC slab, respectively. It is important to note that helium ions beams typically have improved sensitivity than electron beams. Therefore, the dose requirement for helium is ~100 times smaller than electron beams [77]. This can potentially lead to much faster lithography during the mold fabrication procedure [73]. The focused helium ions have 30 kV energy and the current of the beam is 0.2 pA. A 10 μm diameter aperture is used with a spot size of 5. The spot of the focused ion beam has a diameter set by default as 0.5 nm by the equipment Zeiss OrionFab. The spacing between each spot is set as by 6 nm, and the exposure time for each spot is 1.2 μs. Therefore, the line scan speed is around 5 mm/s. Peforming HIL on a 600 × 600 μm^2 size area to produce line grating with 50% duty cycle takes around 1.67 h.

2.2. Simulation and characterization for photonic crystal slab surface

To demonstrate the function of the fabricated PC biosensor, we characterized a few examples of 1D (Figs. 3 and 4) and 2D (Fig. 5) PC slabs. Fig. 3(a,b) show the simulation (blue curve) and experimental (red curve) results for a 1D nanograting PC slab surface. The PC is nanoreplicated from a HIL-fabricated nanomold with a period of ~400 nm and grating-width of ~240 nm. The simulation is carried out (with a commercial software (FDTD Solutions, Lumerical, Inc.) using the Finite-Difference Time-Domain (FDTD) method (FDTD Solutions, Lumerical, Inc.). The simulation is performed with

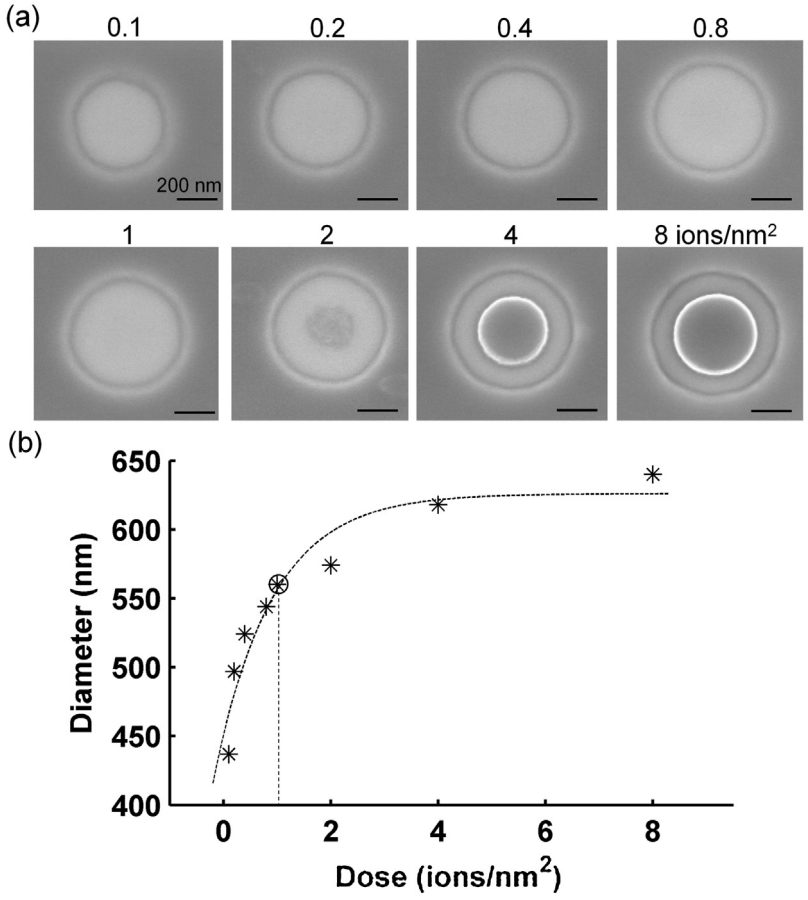

Fig. 1. Helium Ion Lithography Dose Response for PMMA Mold. (a) SEM images of developed PMMA resists exposed with ~400 nm diameter circle with different amount of He^+ doses. (b) Measured diameter of circles exposed at different He^+ does. The diameters of the circles initially increase linearly with increasing doses, then gradually saturate around 650 nm diameter.

the light source polarized as Transverse Magnetic (TM) mode and the parameters of the nanostructure are as follows: the refractive index of the UVCP nanograting structure is 1.46, the grating depth is ~100 nm, the grating period is ~400 nm, and the duty cycle is ~40%. The refractive index of the TiO_2 slab (on the top of the UVCP) is 2.4 and the slab thickness is chosen as ~86 nm to support the resonance modes at the desired peak wavelength. The simulated and measured spectra of the PC surface is plotted in Fig. 3 (a, b) for different resonance conditions: (a) in air (environment refractive index is 1) and (b) in water (environment refractive index is 1.333), respectively. The characterization experiment is performed in a linear optical transmission/reflection setup with an illuminating source from collimiated white light. The FDTD simulation results predicted a narrowband reflectance on the proposed 1D nanograting PC structure, which is verified by the experimental results. The quality factor (Q-factor) is a dimensionless characterization parameter to describe the damping properties of a resonator and is defined as a resonator's bandwidth relative to its center wavelength in this work. The Q-factor of the fabricated 1D PC slab surface is measured as Q_{TM} = ~194.2, Q_{TE} = ~90.7 in water. This Q-factor is slightly higher than the 1D PC slab surface that we fabricated using E-beam lithography and NIL previously in our lab (Q_{TM} = ~160 and Q_{TE} = ~72 in water).

One example spectra of the PC (in a water environment) with a TM polarized light source can be seen in Fig. 3(b). The blue curve demonstrates that the PC structure has a peak wavelength value (PWV) of ~631.82 nm in simulation, and the red curve shows that the PWV is ~632 nm in the experimental measurement. This peak resonance can also be observed in the simulation results in the near-field of electromagnetic field distributions. Fig. 3 (c, d) show the evanescent-field calculated as 2D simulation maps at two different wavelengths (on/off resonances wavelengths are ~632/637 nm). The figure clearly shows that the highest intensity of the evanescent field at the on-resonance wavelength of ~632 nm (Fig. 3 (c)) is much higher than that of the off-resonance wavelength of ~637 nm (Fig. 3 (d)) in air.

The resonance wavelength of the PC can be tuned by varying the refractive indices of the background materials (exposed within the evanescent field region) at different light incident angles. As shown in the dispersion relation maps in Fig. 4, a photonic bandgap is predicted in simulation (Fig. 4 (a)) and observed in experiments (Fig. 4(b)) for TM polarization in air environment. A similar phenomenon can be found in the measured spectra maps in TE polarization as shown in a 3D plot in Fig. 4(c).

2.3. Functional test for photonic crystal biosensor

As shown in Fig. 2 (e, f), our HIL-NIL approach can fabricate not only 1D nanograting patterns but also 2D nanohole patterns. An example of PC slab (2D nanohole) biosensor is fabricated using the HIL-NIL approach with ~400 nm pitch and used to investigate the sensing performance. The PC slab biosensor is characterized for the TE polarization mode with a mixture of Dimethyl sulfoxide (DMSO) and water solutions exposed on the surface. As shown in Fig. 5(a), the reflectance spectra are measured on the PC surface with different concentrations (0%, 1%, 2%, 4%, 6%, 8%, 10%) of DMSO solutions (different effective refractive indices). Fig. 5 (b) represents the peak intensity value (PIV) sensitivity curve linearly fitted from

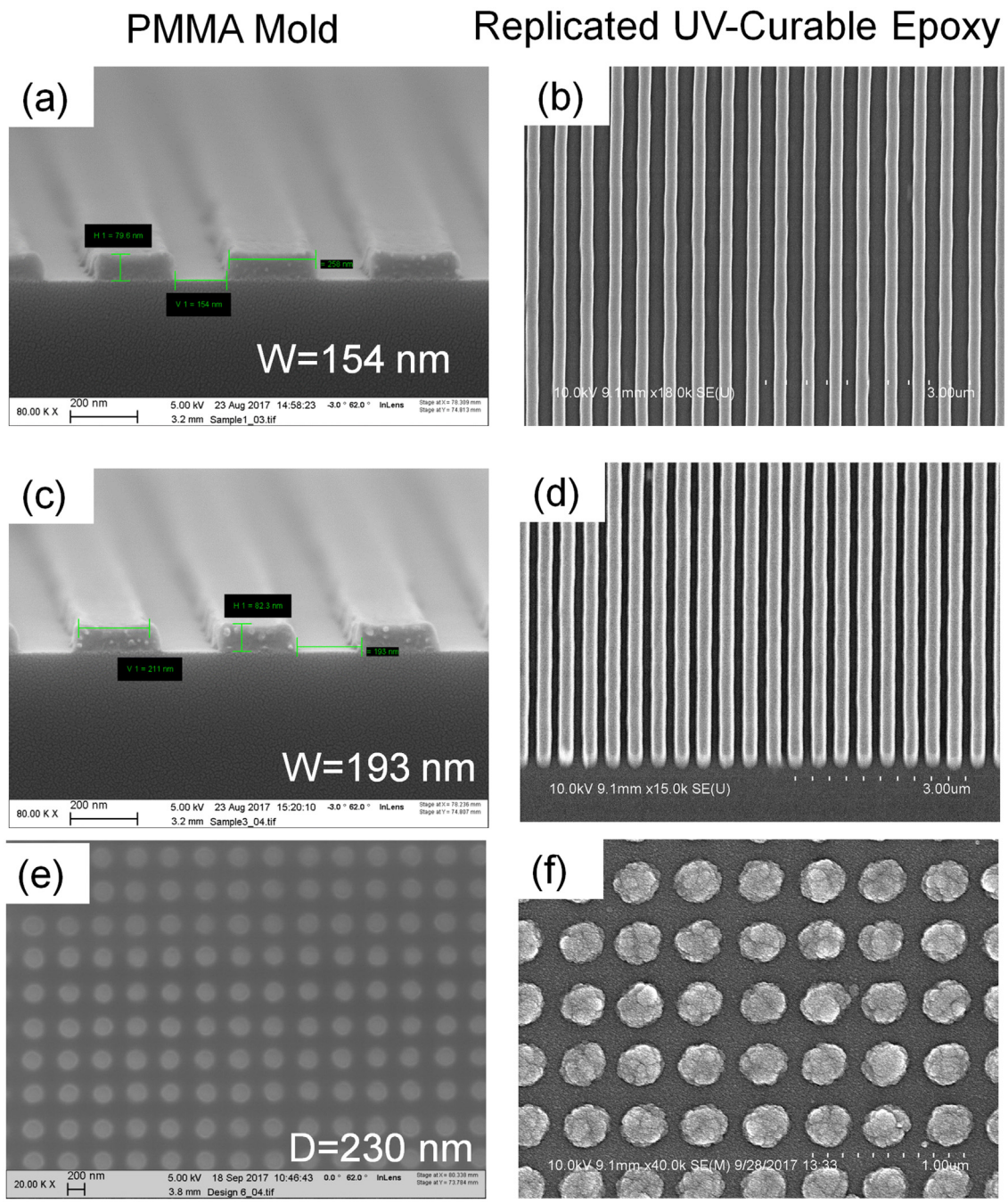

Fig. 2. SEM images of PMMA nanograting molds of three different PCs as well as replicated UV-Epoxy structures. PMMA mold (a,c) and replicated UV-Epoxy polymer nanograting (b, d) for different duty cycles of 1D nanogratings photonic crystal slab surfaces. PMMA mold (e) and replicated UV-Epoxy polymer nanograting (f) for 2D nanoholes photonic crystal slab surfaces.

the experimental measurement. It shows that the PIV can successfully distinguish the different concentrations of DMSO solutions. Not only the peak intensity but also the peak wavelength of the reflection spectra measured on PC surface can be used as a label-free sensing signal. Fig. 5 (c, d) shows the extracted peak wavelength value (PWV) sensitivity curve linearly-fitted from the simulation and experimental results. Both the simulation and experimental results demonstrate that the PWV measured on the PC surface follows the variation of effective refractive index, and therefore the fabricated PC slab surface successfully functions as a label-free optical biosensor.

2.4. Advantages of HIL-NIL fabrication strategy

There are two major challenges during the PC fabrication process: (1) within chip (the same nanostructure needs to be preserved between periods): this requires enough fabrication precision to prevent optical scattering losses blurring the crystal properties of the PC. In fact, this is challenging for any periodic nanostructure fabrication, including PC, since each period has to be identical to preserve the narrow bandwidth and quality factor. (2) Between chips (the same nanostructure needs to be preserved between chips): the PC fabrication process requires high precision so that the designed nanopatterns can be robustly mass-produced to guarantee that each PC chip shares the same nanophotonics function. The

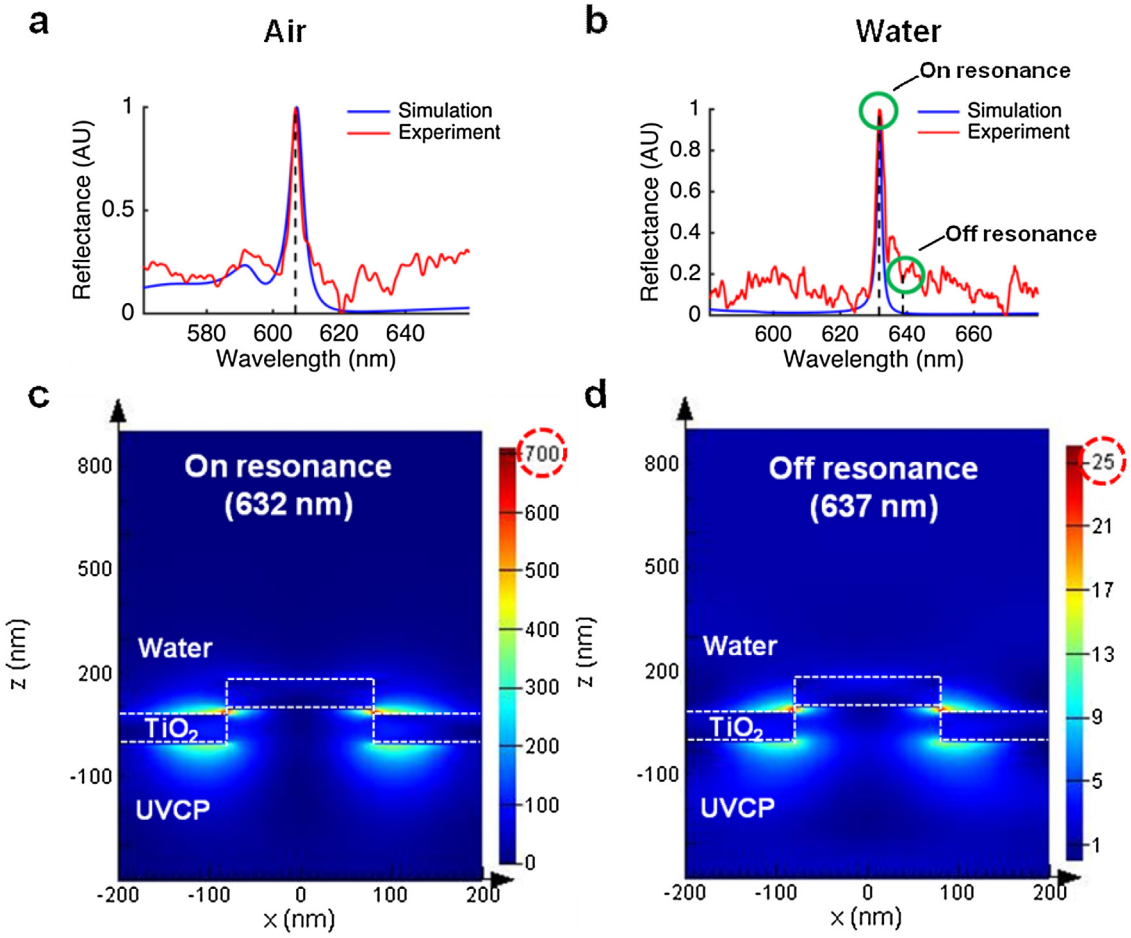

Fig. 3. Reflectance and E-field Intensity of 1D nanograting PC under different resonance conditions. The blue curves are the simulation results and the red curves are the experimental results for the following conditions: (a) Air-TM; (b) Water-TM. Cross-section view of the simulated E-field intensities for on-resonance (c) and off-resonance (d) of Water-TM. (For interpretation of the references to colour in this figure legend, the reader is referred to the web version of this article).

first challenge can be overcome by HIL due to its small beam spot (~0.5 nm) and minimum proximity effect. The second challenge can be solved by using NIL due to its excellent reliability, repeatability and resolution. The fabriation errors within a chip originate from the ion beam current fluctuations, the stage stability, the environment noise, and the sensitivity of resist to exposure. The fabriation error between chips fabricated by NIL can be attributed to the gradual mechanical wear of the mold, the uniformity of the epoxy materials, the UV light intensity, and the thickness of the epoxy. The "between chips error" has been reported to be 0.1% [78] for epoxy mold fabricated with NIL and the "within chip error" in our work is measured to be 0.68% for a matrix of 324 circular nano-partterns (as shown in Supplementary Figure 1). Moreover, our strategy of combining HIL and NIL also allows other components such as an optical waveguide and electronic circuits to be fabricated on the same chip as the PCs to achieve integration of photonic processing with electronic processing and improve the optical processing efficiency and optical communications efficiency both within a chip and between chips. Recently, HIL has demonstrated the cability of 3D nanopattern generation and can be promising in constructing even 3D photonic crystals fabrications [73].

3. Materials and methods

Fig. 6 shows the two major phases to fabricate the PC slab biosensors: Phase (I) consists of generating the nanopatterns on the mold using HIL (Fig. 6 (a–c)). The procedure in this phase can be further decomposed into three sub-steps. First, 495 PMMA A2 resist is spin-coated at 1000 RPM for preparing a ~100 nm thin film and prebaked on a 180 °C hotplate for 90 s (step (a)). Second, 30 kV focused helium ion beams are used to expose nanopatterns within a 600 μm × 600 μm area using a helium ion microscope (OrionFab, Zeiss). The exposed patterns are 1500 identical rectangles 600 μm long with specified widths (step (b)). The helium ion current is 0.2 pA (a 10 μm diameter aperture is used with a spot size of 5). The dwelling time and the dose can be chosen as needed during the exposure experiment (e.g., dwelling time of 1.2 μs and dose of 0.18 ions/nm^2 is selected in this work). After helium ion exposure, the sample is dipped into a 50 mL mixture of IPA:DI Water (Isopropyl alcohol: deionized water) with 7:3 vol ratio at room temperature for 5 min to dissolve exposed PMMA and render PMMA nanograting structures (step (c)).

Phase (II) is the nanoreplica molding process (NIL) to transform the structures from the nanopatterned mold to chips (Fig. 6 (d–f)). In this phase, the PMMA nanograting surface is used as a mold to replicate a UV-curable epoxy material (step (d)). The liquid UV-curable epoxy polymer is applied on top of the mold and exposed to UV light. Once cross-linked by the UV radiation, the UV-cured epoxy polymer is solidified with a negative-patterned nanograting structure and detached from the mold (step (e)). Finally, a ~86 nm thick TiO_2 film is sputtered onto the UV epoxy to serve as the light wave confinement layer on the photonic crystal slab (step (f)). This process is relatively simple for making a photonic crystal device as it eliminates the etching processes.

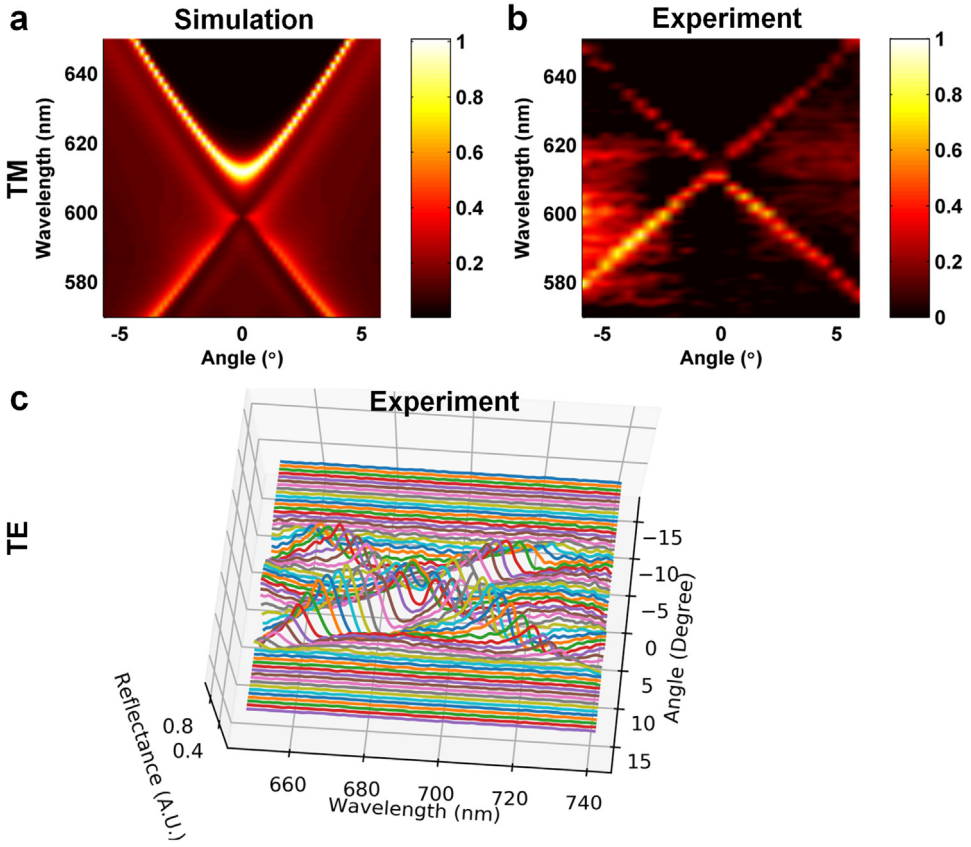

Fig. 4. Dispersion relation maps of 1D nanograting PC under different resonance conditions. (a) Simulation-TM; (b) Experiment-TM; (c) 3D plot the spectra of Experiment-TE.

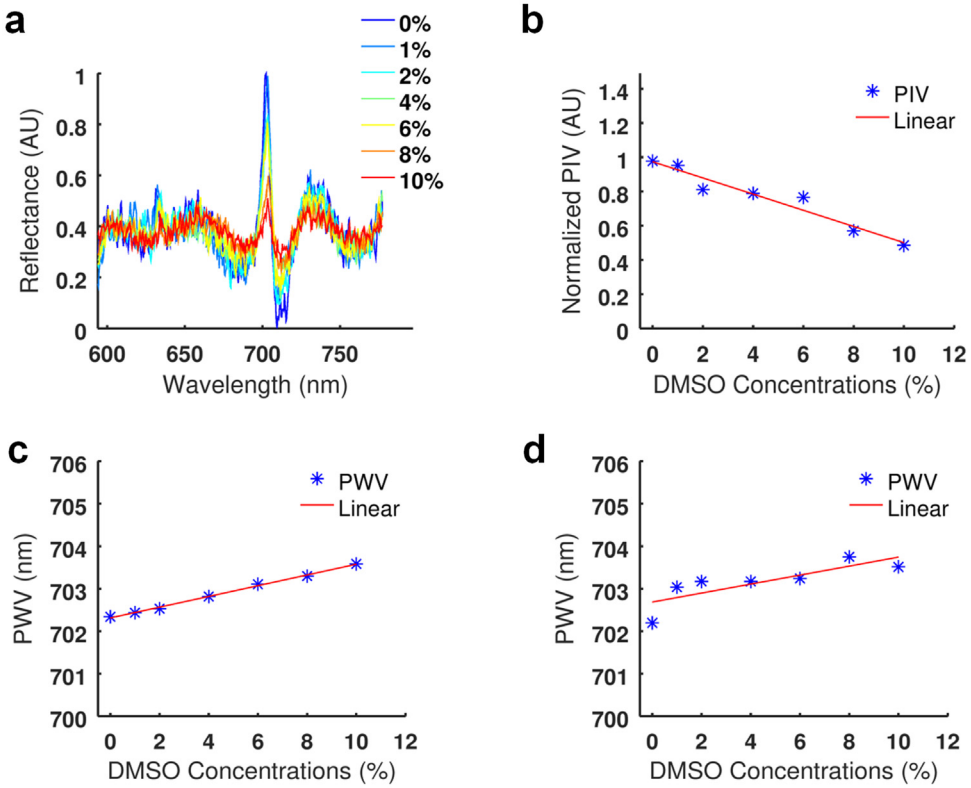

Fig. 5. Reflectance spectra, peak intensity values (PIVs), and peak wavelength values (PWVs). The spectra are measured on a 2D nanohole PC slab surface with different concentrations of DMSO solutions (0%, 1%, 2%, 4%, 6%, 8%, 10%). (a) Reflectance spectra measured in experiment. (b) PIV Sensitivity curve linearly fitted from the experimental results. (c) PWVs sensitivity curve linearly fitted from the simulation results. (d) PWVs sensitivity curve linearly fitted from the experimental results.

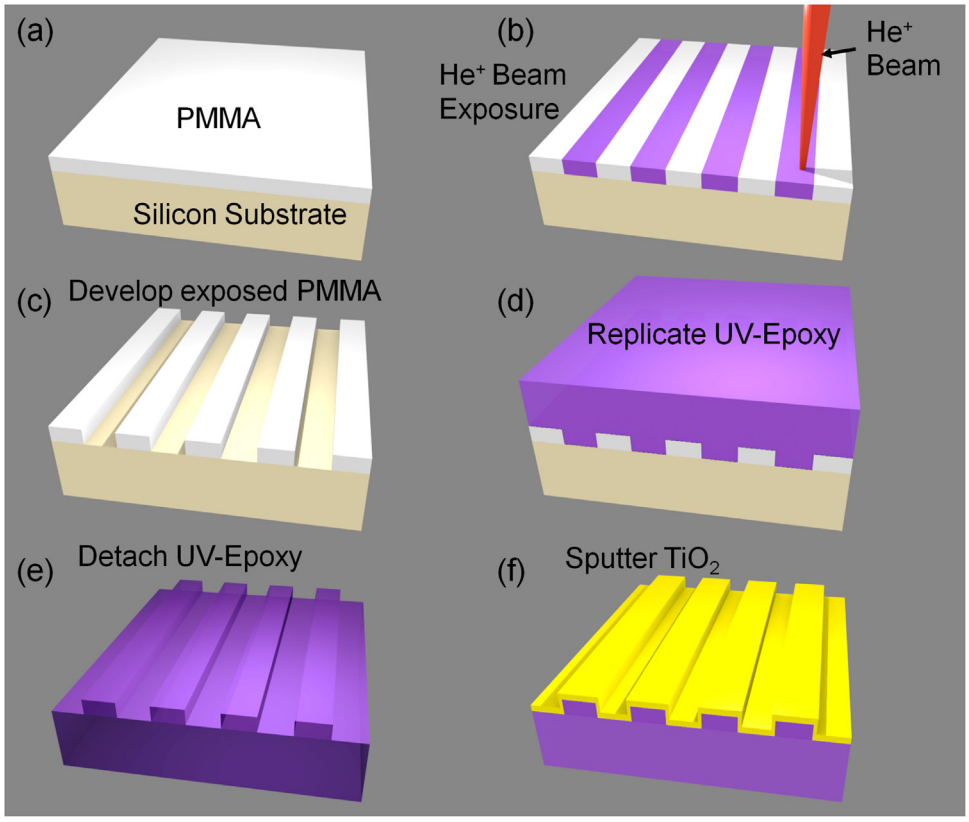

Fig. 6. Photonic Crystal Biosensor Major Fabrication Steps. (a) Spincoat PMMA resist and prebake; (b) He^+ ion exposure with desired patterns; (c) Develop; (d) Replicate the liquid UV-curable Epoxy polymer with the patterned PMMA resist as the mold; (e) Detach the solidfied UV-curable epoxy polymer from the mold; (f) Sputter TiO_2 on top.

4. Conclusions

This work has demonstrated a novel fabrication method of photonic crystal slab surface by combining both helium ion lithography and nanoimprint lithography. The basic properties and the function of the photonic crystal biosensors have been predicted in the simulation and demonstrated in the experimental results to prove the concept. The 1D nanograting and 2D nanohole patterned photonic crystal slab surface have been fabricated and verified as functional label-free biosensors. As such, the framework presented here provides a technological potential for mass-production fabrication of nanostructured surface biosensors and we believe that this approach can also be applied to many other nanotechnology applications in the future.

Contributions

Huan Hu performed the helium ion lithography and fabricated the grating molds. Yue Zhuo fabricated the PC slabs using the molds, characterized the PC slabs and performed the functional test. Yunfei Wang completed one part of the lithography process. Thibault Marin helped with the functional experiment data processing. Huan Hu and Yue Zhuo initiated the idea and wrote the manuscript together. Meng Lu provided very meaningful discussions and helped to prepare the manuscript.

Declaration of Competing Interest

The authors declare no competing financial interests.

Acknowledgments

This work was supported in part by the Zhejiang University/University of Illinois at Urbana-Champaign Institute, and was led by Principal Supervisor Huan Hu. This work was also supported by the Beckman Institute Postdoctoral Fellowship at University of Illinois. The content is solely the responsibility of the authors and does not necessarily represent the official views of the Beckman Institute and ZJUI. The authors would like to thank the Nano Sensor Groups (NSG), staff in Micro and Nanotechnology Laboratory (MNTL), the Center for Innovative Instrumentation Technology (CiiT) at University of Illinois at Urbana-Champaign for their support. The work is also funded by the Tang's foundation.

Appendix A. Supplementary data

Supplementary material related to this article can be found, in the online version, at doi:https://doi.org/10.1016/j.sna.2019.07.017.

References

[1] A. Hessel, A.A. Oliner, A New theory of Wood's anomalies on optical gratings, Appl. Opt. 4 (October) (1965) 1275–1297.
[2] L. Mashev, E. Popov, Diffraction efficiency anomalies of multicoated dielectric gratings, Opt. Commun. 51 (September) (1984) 131–136.
[3] E. Popov, et al., Theoretical study of the anomalies of coated dielectric gratings, Optica Acta 33 (December) (1986) 607–619.
[4] E. Yablonovitch, Inhibited spontaneous emission in solid-state physics and electronics, Phys. Rev. Lett. 58 (May) (1987) 2059–2062.
[5] S. John, Strong localization of photons in certain disordered dielectric superlattices, Phys. Rev. Lett. 58 (June) (1987) 2486–2489.
[6] R. Magnusson, S.S. Wang, New principle for optical filters, Appl. Phys. Lett. 61 (August) (1992) 1022–1024.

[7] S. Fan, et al., High extraction efficiency of spontaneous emission from slabs of photonic crystals, Phys. Rev. Lett. 18 (April) (1997) 3294–3297.
[8] J.D. Joannopoulos, et al., Photonic crystals: putting a new twist on light, Nature 386 (March) (1997) 143–149.
[9] S.G. Johnson, et al., Guided modes in photonic crystal slabs, Physical Review B 60 (August) (1999) 5751–5758.
[10] H. Kikuta, et al., Refractive index sensor with a guided-mode resonant grating filter, Proc. SPIE 4416 (June) (2001) 219–222.
[11] S.H. Fan, J.D. Joannopoulos, Analysis of guided resonances in photonic crystal slabs, Physical Review B 65 (June) (2002).
[12] B.T. Cunningham, et al., A plastic colorimetric resonant optical biosensor for multiparallel detection of label-free biochemical interactions, Sens. Actuators B 85 (2002) 219–226.
[13] B. Cunningham, et al., Enhancing the surface sensitivity of colorimetric resonant optical biosensors, Sensors and Actuators B-Chemical 87 (December) (2002) 365–370.
[14] F. Villa, et al., Photonic crystal sensor based on surface waves for thin-film characterization, Opt. Lett. 27 (April) (2002) 646–648.
[15] B. Lin, et al., A label-free optical technique for detecting small molecule interactions, Biosens. Bioelectron. 17 (September) (2002) 827–834.
[16] B.T. Cunningham, et al., Label-Free assays on the BIND system, J. Biomol. Screening 9 (2004) 481–490.
[17] C.J. Choi, B.T. Cunningham, Single-step fabrication and characterization of photonic crystal biosensors with polymer microfluidic channels, Lab Chip 6 (October) (2006) 1373–1380.
[18] Y. Fang, et al., Resonant waveguide grating biosensor for living cell sensing, Biophys. J. 91 (September) (2006) 1925–1940.
[19] B.T. Cunningham, L. Laing, Microplate-based, label-free detection of biomolecular interactions: applications in proteomics, Expert Rev Proteomics 3 (June) (2006) 271–281.
[20] N. Skivesen, et al., Photonic-crystal waveguide biosensor, Opt. Express 15 (March) (2007) 3169–3176.
[21] V.N. Konopsky, E.V. Alieva, Photonic crystal surface waves for optical biosensors, Anal. Chem. 79 (June) (2007) 4729–4735.
[22] J.D. Joannopoulos, et al., Photonic Crystals: Molding the Flow of Light, second edition, Princeton University Press, Princeton, New Jersey, 2008.
[23] Y. Fang, et al., Label-free cell-based assays for GPCR screening, Comb. Chem. High Throughput Screen. 11 (June) (2008) 357–369.
[24] Y.B. Guo, et al., Sensitive molecular binding assay using a photonic crystal structure in total internal reflection, Opt. Express 16 (August) (2008) 11741–11749.
[25] Y. Nazirizadeh, et al., Spatially resolved optical characterization of photonic crystal slabs using direct evaluation of photonic modes, in: Gremany Freiburg (Ed.), IEEE Proc. Optical MEMs and Nanophotonics, 2008, pp. 112–113.
[26] V.N. Konopsky, E.V. Alieva, Optical biosensors based on photonic crystal surface waves, Methods Mol. Biol. 503 (2009) 49–64.
[27] B.T. Cunningham, Photonic crystal surfaces as a General purpose platform for label-Free and fluorescent assays, JALA Charlottesv Va 15 (April) (2010) 120–135.
[28] M. El Beheiry, et al., Sensitivity enhancement in photonic crystal slab biosensors, Opt. Express 18 (October) (2010) 22702–22714.
[29] R. Magnusson, et al., Resonant photonic biosensors with polarization-based multiparametric discrimination in each channel, Sensors 11 (January) (2011) 1476–1488.
[30] Y. Zhuo, et al., Single nanoparticle detection using photonic crystal enhanced microscopy, Analyst 139 (2014) 1007–1015.
[31] Y. Nazirizadeh, et al., Low-cost label-free biosensors using photonic crystals embedded between crossed polarizers, Opt. Express 18 (August) (2010) 19120–19128.
[32] C. Jamois, et al., New concepts of integrated photonic biosensors based on porous silicon, in: P.A. Serra (Ed.), Biosensors - Emerging Materials and Applications, InTech, Rijeka, Croatia, 2011.
[33] J.O. Grepstad, et al., Photonic-crystal membranes for optical detection of single nano-particles, designed for biosensor application, Opt. Express 20 (March) (2012) 7954–7965.
[34] Y. Nazirizadeh, et al., Photonic crystal slabs for surface contrast enhancement in microscopy of transparent objects, Opt. Express 20 (June) (2012) 14451–14459.
[35] D. Threm, et al., Photonic crystal biosensors towards on-chip integration, J. Biophotonics 5 (August) (2012) 601–616.
[36] J. Carbonell, et al., Radial photonic crystal for detection of frequency and position of radiation sources, Sci. Rep. 2 (2012) 558.
[37] S. Pal, et al., 1-D and 2-D photonic crystals as optical methods for amplifying biomolecular recognition, Anal. Chem. 84 (September) (2012) 8900–8908.
[38] B. Troia, et al., Photonic crystals for optical sensing: a review, in: V.M.N. Passaro (Ed.), Advances in Photonic Crystals, InTech, Rijeka, Croatia, 2013.
[39] J. Shin, et al., Fast response photonic crystal pH sensor based on templated photo-polymerized hydrogel inverse opal, Sens. Actuators, B 150 (2010) 183–190, 09/21/ 2010.
[40] N.L. Privorotskaya, et al., Sensing micrometer-scale deformations via stretching of a photonic crystal, Sens. Actuators, A 161 (2010) 66–71, 06/01/ 2010.
[41] Y. Yang, et al., Photonic crystal stress sensor with high sensitivity in double directions based on shoulder-coupled aslant nanocavity, Sens. Actuators, A 193 (2013) 149–154, 04/15/ 2013.
[42] Y. Xia, et al., Self-assembly approaches to Three-dimensional photonic crystals, Adv. Mater. 13 (March) (2001) 409–413.
[43] V.N. Astratov, et al., Optical spectroscopy of opal matrices with CdS embedded in its pores: quantum confinement and photonic band gap effects, Il Nuovo Cimento D 17 (November) (1995) 1349–1354.
[44] A. Blanco, et al., Large-scale synthesis of a silicon photonic crystal with a complete three-dimensional bandgap near 1.5 micrometres„ Nature 405 (2000) 437.
[45] D. Segura, et al., Effect of fabrication tolerances in macroporous silicon photonic crystals, Sens. Actuators, A 264 (2017) 172–179, 09/01/ 2017.
[46] G. Subramania, S.Y. Lin, Fabrication of three-dimensional photonic crystal with alignment based on electron beam lithography, Appl. Phys. Lett. 85 (September) (2004), 2004.
[47] D. Freeman, et al., Fabrication of planar photonic crystals in a chalcogenide glass using a focused ion beam, Opt. Express 13 (April) (2005) 3079–3086.
[48] S.H.G. Teo, et al., Hole-type two-dimensional photonic crystal fabricated in silicon on insulator wafers, Sens. Actuators, A 133 (2007) 388–394, 02/12/ 2007.
[49] M. Li, et al., Photonic bandpass filter for 1550 nm fabricated by femtosecond direct laser ablation, Appl. Phys. Lett. 83 (2003) 216–218.
[50] L. Rayleigh, XXVI. On the remarkable phenomenon of crystalline reflexion described by prof. Stokes, The London, Edinburgh, and Dublin Philosophical Magazine and Journal of Science 26 (1888) 256–265, 09/01 1888.
[51] E. Yablonovitch, et al., Photonic band structure: the face-centered-cubic case employing nonspherical atoms, Phys. Rev. Lett. 67 (October) (1991) 2295–2298.
[52] H.S. Sözüer, J.P. Dowling, Photonic band calculations for woodpile structures, J. Mod. Opt. 41 (1994) 231–239, 02/01 1994.
[53] K.M.M. Ho, et al., Photonic band gaps in three dimensions: New layer-by-layer periodic structures, Science Direct 89 (1994).
[54] S. Fan, et al., Design of three-dimensional photonic crystals at submicron lengthscales, Appl. Phys. Lett. 65 (1994) 1466–1468.
[55] C.C. Cheng, A. Scherer, Fabrication of photonic band-gap crystals, J. Vac. Sci. Technol. B 13 (1995) 2696–2700.
[56] N. Susumu, et al., New realization method for Three-dimensional photonic crystal in optical wavelength region, Jap. J. Appl. Phys. 35 (1996) L909.
[57] S.G. Romanov, et al., Enhancement of the photonic gap of opal-based three-dimensional gratings, Appl. Phys. Lett. 70 (1997) 2091–2093.
[58] G. Feiertag, et al., Fabrication of photonic crystals by deep x-ray lithography, Appl. Phys. Lett. 71 (1997) 1441–1443.
[59] S.Y. Lin, et al., A three-dimensional photonic crystal operating at infrared wavelengths, Nature 394 (1998) 251.
[60] R.D. Meade, et al., Novel applications of photonic band gap materials: low-loss bends and high Q cavities, J. Appl. Phys. 75 (1994) 4753–4755.
[61] P.L. Gourley, et al., Optical properties of two-dimensional photonic lattices fabricated as honeycomb nanostructures in compound semiconductors, Appl. Phys. Lett. 64 (1994) 687–689.
[62] M. Boroditsky, et al., Analysis of photonic crystals for light-emitting diodes using the finite-difference time domain technique, in: Optoelectronics and High-Power Lasers and Applications, 1998, p. 7.
[63] P.R. Villeneuve, et al., Three-dimensional photon confinement in photonic crystals of low-dimensional periodicity, IEE Proc. Optoelectron. 145 (1998) 384–390.
[64] B. D'Urso, et al., Modal reflectivity in finite-depth two-dimensional photonic-crystal microcavities, J. Opt. Soc. Am. A 15 (1998) 1155–1159, 03/01 1998.
[65] M. Kanskar, et al., Observation of leaky slab modes in an air-bridged semiconductor waveguide with a two-dimensional photonic lattice, Appl. Phys. Lett. 70 (1997) 1438–1440.
[66] R. Coccioli, et al., Smallest possible electromagnetic mode volume in a dielectric cavity, IEE Proc. Optoelectron. 145 (1998) 391–397.
[67] T.F. Krauss, et al., Two-dimensional photonic-bandgap structures operating at near-infrared wavelengths, Nature 383 (1996) 699.
[68] Y. Zhuo, B. Cunningham, Label-Free biosensor imaging on photonic crystal surfaces, Sensors 15 (2015) 21613.
[69] Y. Zhuo, et al., Quantitative imaging of cell membrane-associated effective mass density using photonic crystal enhanced microscopy (PCEM), Prog. Quantum Electron. 50 (2016) 1–18, 11/01/ 2016.
[70] Y. Zhuo, et al., Quantitative analysis of focal adhesion dynamics using photonic resonator outcoupler microscopy (PROM), Light: Sci. Appl. 7 (2018).
[71] D. Winston, et al., Scanning-helium-ion-beam lithography with hydrogen silsesquioxane resist, J. Vac. Sci. Technol. B 27 (2009) 2702–2706.
[72] W.-D. Li, et al., Combined helium ion beam and nanoimprint lithography attains 4 nm half-pitch dense patterns, J. Vac. Sci. Technol. B 30 (2012) 06F304.
[73] X. Shi, et al., Proximity Effect Quantification and Dose Optimisation for High Resolution Helium Ion Beam Lithography, 2015.
[74] W. Wu, et al., Sub-10 nm nanoimprint lithography by wafer bowing, Nano Lett. 8 (2008) 3865–3869, 11/12 2008.
[75] F. Hua, et al., Polymer imprint lithography with molecular-scale Resolution, Nano Lett. 4 (2004) 2467–2471, 12/01 2004.
[76] M.D. Austin, et al., Fabrication of 5nm linewidth and 14nm pitch features by nanoimprint lithography, Appl. Phys. Lett. 84 (2004) 5299–5301.
[77] E. van der Drift, D.J. Maas, Helium ion lithography, in: M. Stepanova, S. Dew (Eds.), Nanofabrication: Techniques and Principles, Springer Vienna, Vienna, 2012, pp. 93–116.

[78] N. Ganesh, B.T. Cunningham, Photonic-crystal near-ultraviolet reflectance filters fabricated by nanoreplica molding, Appl. Phys. Lett. 88 (2006), 071110.

Biographies

Yue Zhuo is a Deutsch Research Fellow at Harvard Medical School -Massachusetts General Hospital. Her research interests are photonic devices, new imaging technology and their applications in biomedical field.

Huan Hu is a tenure-track assistant professor at the joint institute of Zhejiang University and University of Illinois at Urbana-Champaign. His research is in advanced nanofabrication technology, micro/nano sensors and lab on a chip integrating nanotechnology.

Yifei Wang received his Bachelors' degree in Iowa State University in 2014 and is now a Ph.D. candidate working with Porf. Meng Lu.

Thibault Marin is a Principal Imaging Scientist at Instarecon Inc. His interest are developing new imaging technology and algorithms.

Meng Lu is a tenure-track assistant professor at Iowa State University in Department of Electrical and Computer Engineering and Department of Mechanical Engineering. His research interests are optical sensors for chemical and biological analysis, photonic devices, microfluidics for sensor integration and optical instrumentation.